Properties of velocity field in the vicinity of synthetic jet generator

P Strzelczyk[1] **and P Gil**[1]

[1] Rzeszow University of Technology, al. Powstańców Warszawy 12, Rzeszów, 35-959, Poland

E-mail: piotstrz@prz.edu.pl

Abstract. The paper presents the results of experimental investigation of velocity field in the vicinity of synthetic jet actuator as a function of Stokes number and for constant Reynolds number. A constant temperature hot-wire anemometer with tungsten–platinum coated single wire probe used for the velocity measurements. Synthetic jet flow visualization was presented, especially process of vortex ring development. Synthetic jet velocity profiles were compared with a solution to fully-developed pipe flow with an oscillating pressure gradient.

1. Introduction

Since the end of the last century, the synthetic jet has been the subject of both experimental and numerical investigations, usually under the name "SJ" synthetic jet [4][5] or "ZNMF" zero net mass flux [8][7]. A synthetic jet actuator consists of an oscillating driver and cavity that contains one or more orifice. This driver may be for example a loudspeaker, piezoelectric diaphragm or a mechanical piston. The device is called ZNMF because the integration of the mass flow rate across the orifice over an integer number of cycles is equal to zero. Although there is no net mass transfer to ambient fluid, the ZNMF device has the interesting property of causing a finite amount of momentum transfer to ambient fluid [2].

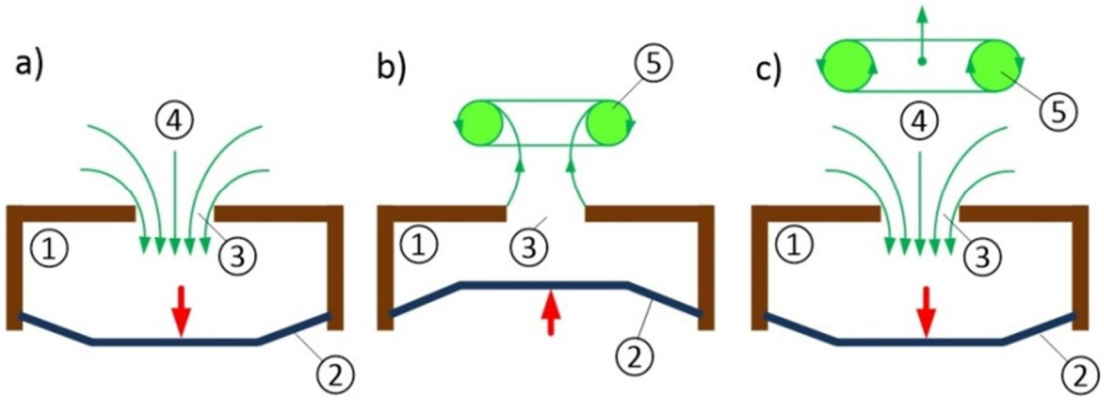

Figure 1. Schematic of a device producing a synthetic jet, a) suction stroke, b) production a vortex ring during ejection stroke c) vortex ring propagates away from the orifice: ① - cavity, ② - diaphragm, ③ - orifice, ④ - ingested fluid, ⑤ - vortex ring

Figure 1 illustrates a typical synthetic jet actuator being operated to producing a synthetic jet. If the diaphragm amplitude ② is high enough, as fluid is expelled through the orifice ③ the boundary layer separates from the wall and, at edge of the orifice, it rolls up to produce a vortex ring ⑤. This vortex ring propagates away from the orifice under its own self-inducted velocity. During the subsequent suction stroke, fluid ④ is drawn into the cavity ① from the surrounding, but the vortex ring has moved sufficiently far from the orifice so as to be relatively unaffected. A new vortex ring is then ejected and the cycle continues, producing a train of vortex rings (fig. 2a). In a time-averaged sense, this behaviour creates a jet-like flow which is synthesized from the ambient fluid (fig. 2b).

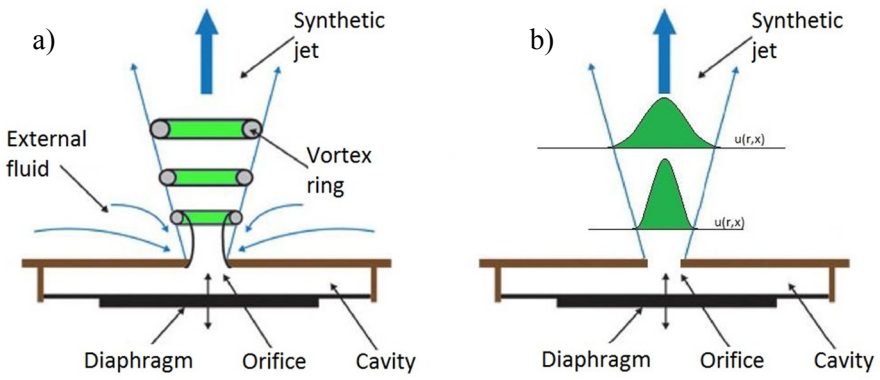

Figure 2. Synthetic jet: a) instantaneous b) time-averaged

Synthetic jet can be used to reduce aerodynamic drag. Reducing aerodynamic drag of bodies was the subject of studies presented in [9]. Synthetic jet actuator mounted in the rear bumper of the Renault Altica has been used to reduction of frontal drag, which at a speed of 130km/h has about 15% lower drag coefficient using the synthetic jet as compared to the case when the synthetic jet generator was switched off [10]. Underwater engines using synthetic jet recently attracted the attention of researchers because they solve the limitations of the current techniques of manoeuvring underwater vehicles [11]. The most promising application of synthetic jet is heat transfer enhancement, both impinging jet as well as in combination with cross-flow [12][13][14]. Synthetic jet actuator have also been used for controlling airflow in aircraft to enhance lift, increase manoeuvrability, control stalls, and reduce noise [15].

2. Experimental setup

a) Synthetic jet actuator

The cavity designed for the purpose of the present study is shown in (fig. 3). It consists of an actuator (loudspeaker STX W.18.200.8.FGX) of 150 mm diameter as the vibrating element fitted to a plexiglas sheet having a centered bore of 150 mm. The loudspeaker nominal impedance is 8Ω, and nominal resonance frequency is 37Hz. The sheets are fastened using four 8 mm bolts. The depth of the cavity H can be adjusted by adding (or removing) plexiglas plates with 150 mm bore in between. Experiments are carried out for three orifice diameters d=9, 15, 24 mm, for one orifice lengths t=5 mm, and for one cavity depths H=20 mm. Working fluid is air. We used a sharp edge orifice. The coordinate system is presented in the (fig. 3). Note that x is axial and r is radial coordinate. All connections between sheets and the loudspeaker have been sealed with silicone paste for the purpose of the leakages elimination. The actual measured resonance frequency of the loudspeaker is 38Hz.

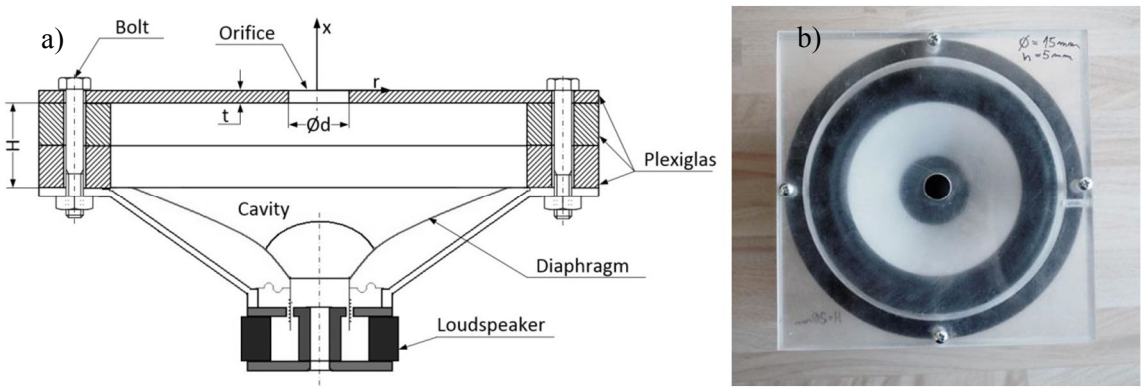

Figure 3. Schematic b) photo of the synthetic jet actuator. Note that *t* is the orifice thickness, *d* is the orifice diameter, *H* is the cavity depth, *r* – radial coordinate, *x* – axial coordinate.

A digital sinusoidal signal generated from LabView application is converted to analog signal with 16-bit 48kHz Realtek ALC889 DAC (Digital to Analog Converter). The LM3886 Texas Instruments amplifier is used to amplify analog signal from DAC and to excite the actuator. Multifunction board (Keithley KPCI-3116A) is used for the purpose of continuous monitoring of the actuator input. The measurement of current in conjunction with voltage gives electrical power supplied to the loudspeaker. The output voltage from the actuator is maintained constant for particular set of experiments. The sampling frequencies of current and voltage measurements are 32 times the actuator excitation frequency.

b) Velocity measurement

A constant temperature hot-wire anemometer (HPA 98 The Strata Mechanics Research Institute) with tungsten–platinum coated single wire probe of sensing element length 1mm is used for the velocity measurements. During calibration conducted in the low-speed wind tunnel of Rzeszow University of Technology, the reference velocity was measured with a Pitot tube connected to the FirstSensor HCLA differential pressure transducer. Measurement points are fitted with a 6th order polynomial curve with a maximum error of 2%. The hot-wire probe is mounted on a two-dimensional manipulator, which allow positioning the probe with an accuracy of 0.01 mm. The sampling frequency was at least 32 times the excitation frequency for all velocity measurements. The Constant temperature anemometer (CTA) probe was 1mm offset from orifice, such procedure turned out to be infeasible due to the hazard of the destruction of hot-wire probe (fig. 4).

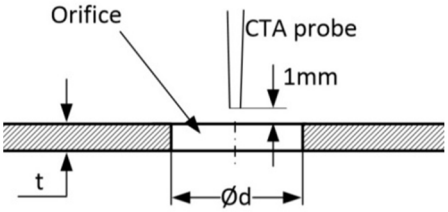

Figure 4. Constant temperature anemometer (CTA) probe position with respect to synthetic jet generator orifice exit

c) Flow visualization

Synthetic jet flow visualisation was realized utilizing light sheet and glycerine vapour (fig. 5). Flow visualization setup consists of: green laser, cylindrical lens, synthetic jet actuator, heaters soaked with glycerine and HD digital camera. Glycerine vapour was illuminated by light sheet.

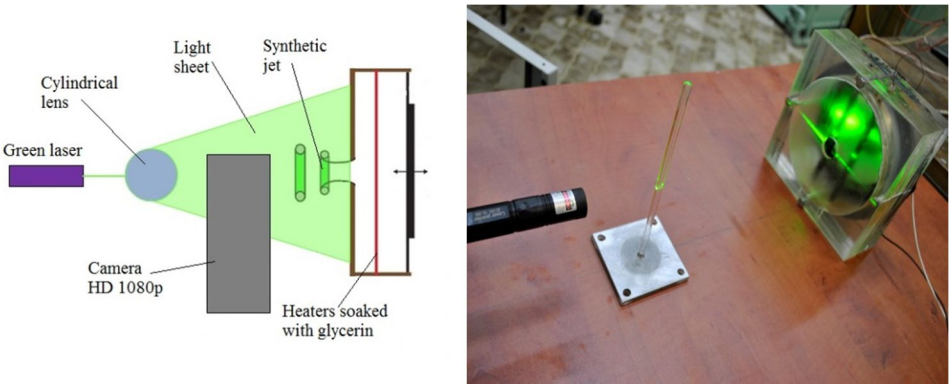

Figure 5. Synthetic jet flow visualization setup: a) schematic, b) photo

The images were captured with a digital camera with a resolution of 1920x1080 HD and 24 frames per second. Due to limitations in the recording speed, a synthetic jet was generated for a constant Stokes number Stk=22, a variable Reynolds number in range, Re = 0 ~ 3340. The uncertainty of the start of the cycle for each series is +/- 1 frame.

3. Data reduction

The Reynolds number is calculated using the procedure given by Holman et al. [1] based on spatial and time-averaged exit velocity during the ejection stroke which is the most common definition:

$$Re = \frac{U \cdot d}{\nu} \tag{1}$$

d- Orifice diameter, *ν*- kinematic viscosity.
Where characteristic velocity *U* was defined as:

$$U = \frac{2}{T} \cdot \frac{1}{A} \int_{A} \int_{0}^{T/2} (u) d\tau dA \tag{2}$$

T – Period, *A* – orifice area, *u* – instantaneous velocity
Root mean square velocity at orifice centreline:

$$U_{RMS.C} = \sqrt{\frac{1}{T} \cdot \int_{0}^{T} u^2 d\tau} \tag{3}$$

Average velocity at orifice centreline:

$$U_{AVG.C} = \frac{1}{T} \cdot \int_{0}^{T} u d\tau \tag{4}$$

The Stokes number is calculated according to the definition given by Holman et al. [1]:

$$Stk = \sqrt{\frac{2\pi f d^2}{\nu}} \tag{5}$$

f – sinusoidal signal frequency
The Strouhal number:

$$Sr = \frac{St^2}{Re} \tag{6}$$

4. Results

a) Flow visualization

In this paper synthetic jet flow visualisation was reduced to one vortex ring development in one period.

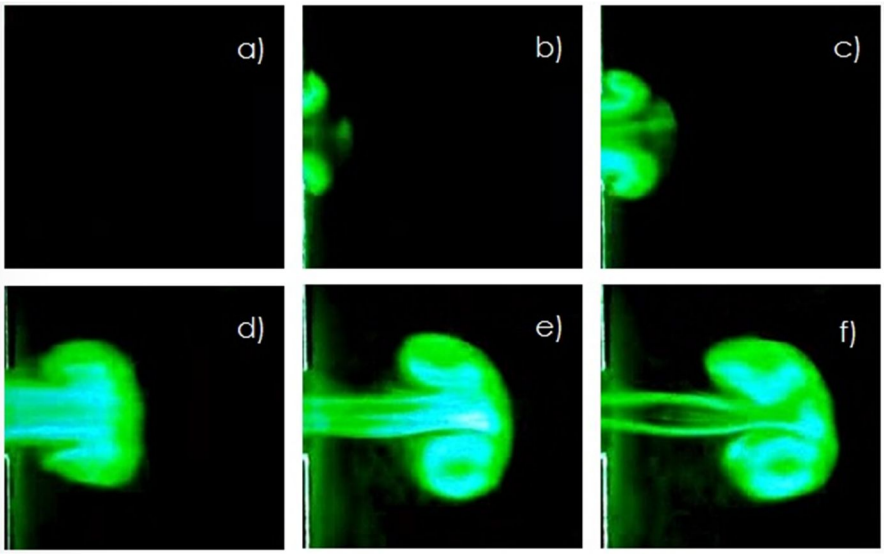

Figure 6. Synthetic jet flow visualization – development of vortex ring

Vortex ring formed in synthetic jet actuator orifice are presented in (fig. 6). Visualization of the formation of the synthetic jet shows the steps to create a coherent structure of the vortex ring. Fluid is expelled through the orifice (fig. 6a). The discharging liquid from an orifice begins to curl on the edge of the orifice (fig. 6b). Initial thin boundary layer ejected from the orifice, it begins to curl into a vortex ring (fig. 6c, d). Ejected fluid from the cavity pushes vortex ring out of the orifice (fig. 6e). On the last picture we can observe fully developed vortex ring (fig. 6f).

b) Axial velocity profile

Synthetic jet close to orifice is dominated by vortex rings which along axial distance increasing their mass and then break down to form a turbulent flow. Instantaneous velocity close to orifice consists of ejection and suction stroke, so time dependent velocity look like sinusoidal wave. Therefore average centreline velocity tends to zero for x/d→0. Average velocity reach maximum at about x/d=2, which indicate that suction stroke has area of influence up there. Root mean square velocity reaches maximum close x/d→0, after which there is appear a plateau.

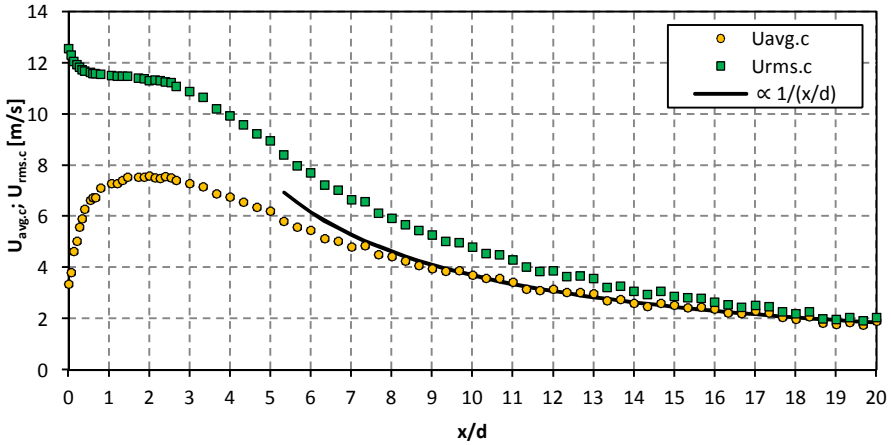

Figure 7. Streamwise variation of time average velocity and momentum synthetic jet velocity at centreline d=15mm; t=5mm; H=40mm; x/d=0÷20; r/d=0, Re=22950, 1/Sr=12.2

Chaudhari et al. [17] has shown that self-similarity of the velocity profile occurs after a distance of 7 times the orifice diameter. Mallison et al. [18] reports a value of 10d and Cater and Soria [19] report a value of 15d based on the mean velocity. The experimental results show that beyond x/d of 9 the velocity indeed decays as x^{-1}, which indicates that the jet is self-similar beyond this distance.

c) Analytical model

The problem of fully-developed pipe flow with an oscillating pressure gradient is the most reasonable exact solution available to model flows emanating from the orifice of synthetic jet actuator.
The nondimensional solution for the radial velocity profile [1]:

$$\frac{u}{u_{max}} = -i \cdot \frac{16}{Stk^2}\left[1 - \frac{J_0\left(\frac{r}{d} \cdot Stk \cdot \sqrt{-i}\right)}{J_0\left(0{,}5 \cdot Stk \cdot \sqrt{-i}\right)}\right] \cdot e^{i\omega\tau} \tag{7}$$

Where: u – velocity, Stk – Stokes number, τ – time, r – radial coordinate, d – orifice diameter, J_0 – zero order Bessel function.
This solution of Navier-Stokes equations shows the velocity profiles during the ejection stroke (fig. 7) for several Stokes number in range Stk=1÷100 obtained from the solution (7). For small values of the Stokes number Stk=1÷8 radial velocity profile is similar to a parabola (fig. 7), representing Poiseuille'a pipe solution. Then, with the increase of the Stokes number Stk>8 it can be seen that the maximum velocity does not occur in the centreline, but shifts to the edges it is known, as Richardson effect [16].

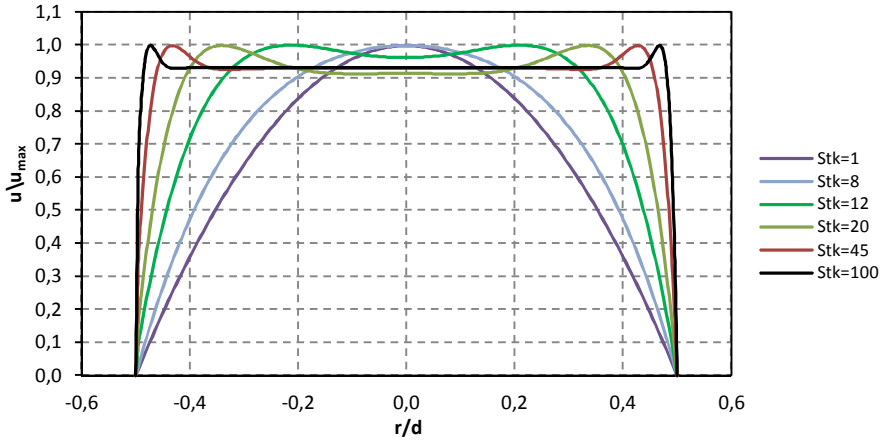

Figure 8. Normalized radial velocity profile vs. normalized radius for several Stokes number

d) Radial velocity profile

For comparison the profiles obtained from the solution of the Navier-Stokes equations (7) for an infinite tube with oscillating pressure gradient, radial velocity profiles of synthetic jet was experimentally studies for three Stokes numbers Stk=8.2; 45.1; 84.8 and constant Reynolds number Re≈4450. The sampling frequency was increased up to 360S/(s·Hz) samples per cycle, measuring and averaging 100 cycles. The sampling frequency has been chosen due to the uncertainty of angular velocity, which in this case is ± 1° for 360° range.

In (fig. 9) shows the synthetic jet radial velocity profile with the velocity profile obtained from the analytical solution (black line). As can be seen, there are discrepancies in the shape of the profile of synthetic jet for maximum velocity during the ejection stroke Φ=300°, and the mathematical model.

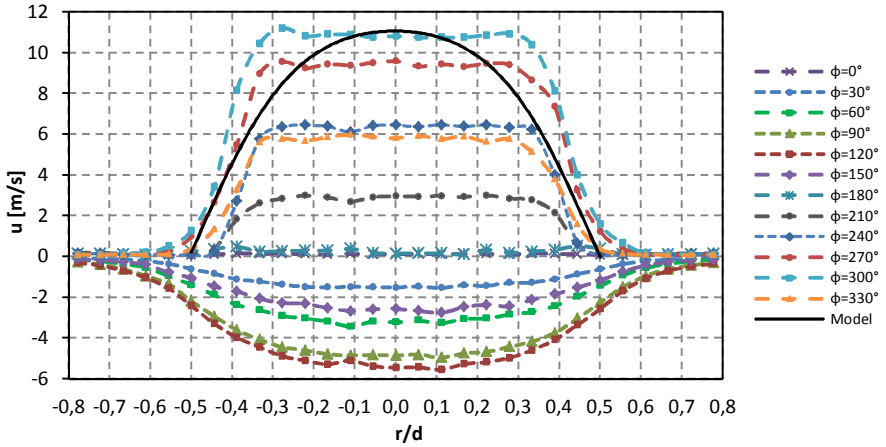

Figure 9. Synthetic jet radial velocity profile vs. normalized radius for Stokes number: Stk=8.2; Re=4334; t=5mm, d=9mm, H=40mm

Differences are due to several reasons; the first is that the radial velocity profiles were measured at the distance 1mm from orifice. Another reason is the finite length of the nozzle which in this case is 5mm (t/d=0.56), compared with an infinite length in the mathematical model may be another cause of the discrepancy.

For the Stokes number Stk=8.2 radial velocity profile obtained from a solution of the mathematical model has a flattened shape of a parabola, with no visible Richardson effect. Synthetic jet velocity profile for Stokes number Stk=8.2 has a much uniform profile with a visible Richardson effect Φ=300 °. Current velocity reaches a maximum of approximately 11m/s in the ejection stroke, while the minimum velocity in the suction stroke reaches about -5.5m/s.

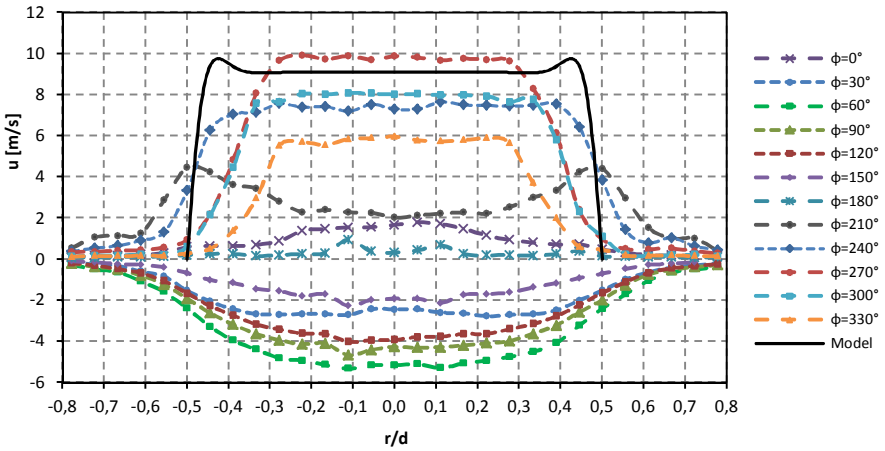

Figure 10. Synthetic jet radial velocity profile vs. normalized radius for Stokes number: Stk=45.1; Re=4687; t=5mm, d=9mm, H=40mm,

In the (fig. 10) velocity profile for the synthetic for Stokes number Stk=45.1 and Reynolds number Re=4687 with the analytical solution for the same number of Stokes number are presented. It can be seen that the profile of the synthetic jet is significantly narrower in comparison to the mathematical model solution. Furthermore there are no Richardson effects for synthetic jet velocity profile for the maximum ejection stroke. It is however clearly visible for Φ=210°. The instantaneous velocity reaches up to 10m/s in a ejection part, while the minimum velocity reaches about -5,3m/s.
In the (fig. 11) velocity profile for the synthetic jet for the Stokes number Stk=84.4 and Reynolds number Re=4458 with the analytical solution for the same Stokes number are presented.

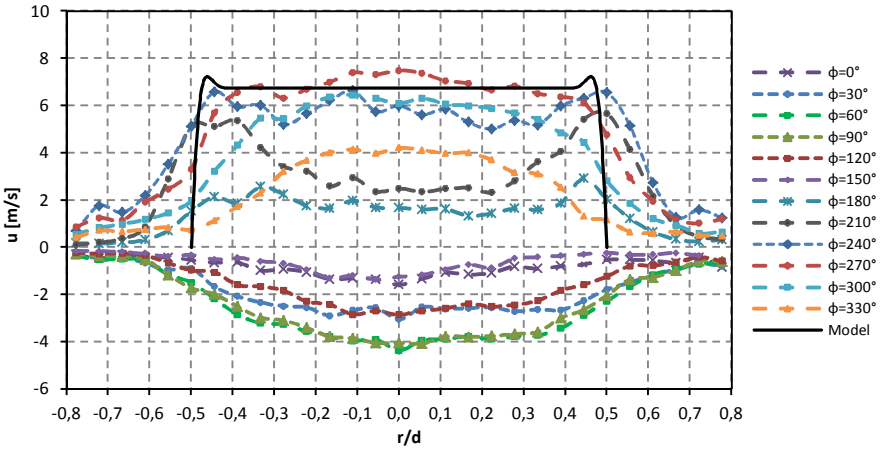

Figure 11. Synthetic jet radial velocity profile vs. normalized radius for Stokes number: Stk=84.8; Re=4458; t=5mm, d=9mm, H=40mm,

It can be seen that the Richardson effect appears at profiles Φ=180°÷240° but does not exist for the maximum velocity at ejection stroke. In addition, the Richardson's effect of synthetic jet is much broader than that implied by the analytical solution. It can be seen that the red line Φ=270° is similar in shape to the profile obtained from a mathematical model. Both models are flat. In contrast, showing significant differences in the width of the profiles during the ejection stroke which is much wider compared to the profile 1, for a low Stokes number. Velocity reaches a maximum of about 7.5 m/s, while the minimum velocity reaches about -4,4m/s.

5. Discussion

Tang et al. [3] made experimental and numerical investigation of flows result from the orifice of synthetic jet actuator. A good agreement between the prediction and the measurement was achieved. For low Stokes number radial velocity profile is remains parabolic, while for high Stokes number it is

more uniform for described solution. Experimental investigated velocity profile behave similarly but only for low Reynolds number, for high Reynolds number are less qualitative compliance.

References

[1] Holman, R., Utturkar, Y., Mittal, R., Smith, B. L., & Cattafesta, L. Formation criterion for synthetic jets. AIAA journal, 43(10), 2005, 2110-2116.
[2] Smith, B. L., and Glezer, A., The Formation and Evolution of Synthetic Jets, Physics of Fluids, Vol. 10, No. 9, 1998, 2281–2297.
[3] Tang H., Zhong S.: Incompressible flow model for synthetic jets actuators, AIAA Journal 44 (4), 2006, 908-912
[4] Jain, M., Puranik, B., & Agrawal, A. (2011). A numerical investigation of effects of cavity and orifice parameters on the characteristics of a synthetic jet flow. Sensors and Actuators A: Physical, 165(2), 351-366.
[5] James, R. D., Jacobs, J. W., and Glezer, A., "A Round Turbulent Jet Produced by an Oscillating Diaphragm," Physics of Fluids, Vol. 8, No. 9, 1996, pp. 2484–249
[6] Mallinson, S. G., Reizes, J. A., and Hong, G., "An Experimental and Numerical Study of Synthetic Jet Flow," The Aeronautical Journal, Vol. 105, No. 1043, 2001, pp. 41–49.
[7] Pack, L. G., and Seifert, A., "Periodic Excitation for Jet Vectoring and Enhanced Spreading," Journal of Aircraft, Vol. 38, No. 3, 2001, pp. 486–495.
[8] Cater, J. E., & Soria, J., "The Evolution of Round Zero-Net-Mass-Flux Jets," Journal of Fluid Mechanics, Vol. 472, 2002, pp. 167–200.
[9] Jeon S., Choi J., Jeon W. P., Choi H., & Park J. (2004). Active control of flow over a sphere for drag reduction at a subcritical Reynolds number. Journal of Fluid Mechanics, 517, 113-129
[10] Renault, Renault Altica: 44MPG Diesel Concept with Active Airflow Management, 2006, http://www.greencarcongress.com/2006/02/renault altica.html.
[11] Mohseni K., (2006). Pulsatile vortex generators for low-speed maneuvering of small underwater vehicles. Ocean Engineering, 33(16), 2209-2223
[12] Gillespie M., Black W., Rinehart C., Glezer A.: Local convective heat transfer from a constant heat flux flat plate cooled by synthetic air jets. ASME Journal of Heat Transfer 128, 2006, s. 990-1000
[13] Gil P., Strzelczyk P.: Porównanie właściwości chłodzących strugi syntetycznej i strugi swobodnej. Zeszyty Naukowe Politechniki Rzeszowskiej 291, Mechanika 87 (2/15), 2015 s.105-117
[14] Timchendo V., Reizes J.A., Leonardi E., Stella F.: Synthetic jet forced convection heat transfer enhancement in micro-channels, International Journal of Numerical Methods for Heat & Fluid Flow 17, 2007, s. 263-283
[15] Glezer A., Amitay M.: Synthetic Jets, Annual Review of Fluid Mechanics 34, 2002, s. 503-529
[16] Richardson E.G., Tyler, E.: The transverse velocity gradients near the mouths of pipes in which an alternating or continuous flow of air is established. The Proceedings of the Physical Society 42 (231), 1929, s. 1-15
[17] Chaudhari, M., Verma, G., Puranik, B., & Agrawal, A. (2009). Frequency response of a synthetic jet cavity. Experimental Thermal and Fluid Science, 33(3), 439-448.
[18] Mallinson, S. G., Reizes, J. A., and Hong, G., "An Experimental and Numerical Study of Synthetic Jet Flow," The Aeronautical Journal, Vol. 105, No. 1043, 2001, pp. 41–49.
[19] Cater, J. E., & Soria, J., "The Evolution of Round Zero-Net-Mass-Flux Jets," Journal of Fluid Mechanics, Vol. 472, 2002, pp. 167–200.